# Robust Mode-Detection Schemes in a Non-stationary Environment

François A. Marshall* David J. Thomson†

**Abstract**

This paper reviews the methods of established mode-detection techniques in the field of multitaper spectrum estimation. The paper presents results of the application of these techniques to the time series of a relative ionospheric opacity meter, an instrument used to measure fluctuations in the opacity of the lower ionosphere to radio waves. The statistical test is robust because of two reasons. First, extraneous measurements in the dataset are replaced by hard-rejection techniques. Second, the test statistic is a spectrum estimator of the component process with the least signal-to-noise ratio, and so its distribution is variance-efficient with respect to a mixture of chi-squared distributions. In the presented analysis, the mode-detection test reveals that a fraction of the noise-like component process of the time series is explicable by periodic phenomena of known origin. In particular, some of the variance of this process is explained by the coupling of solar modes to the radio-emissions opacity of the lower ionosphere.

**Key Words:** Mode, test, multitaper, spectrum, non-parametric, mixture-distribution, quantile, maximum-likelihood, central-limit-theorem,

## 1. Introduction and Methodology

In the problem of mode detection, the field of statistical science is essential because those random modal signals of a system which have low signal-to-noise ratio (SNR) explain a significant fraction of the time-series output, but their presence is obscured by interactions of the phenomenal and detection systems with extraneous processes.

A variety of processes which generate space-physics datasets behave periodically. It is commonly found that harmonic oscillators occur in complicated dynamical systems, where the small oscillations are damped, they are externally forced, and they couple with a large number of other small oscillations of the same system. It is well established in physics that, were the process of interest deterministic, continuous and known at all times, its Fourier transform would reveal all the component oscillators. This is a consequence of an important fact in dynamics: for a system of harmonic oscillators, the normal modes are precisely the coordinates which describe its uncoupled oscillations. This mode-detection scheme is complicated by several factors. For example, it was long supposed that space-physics processes such as measurements of the interplanetary magnetic field revealed turbulent structure in the low-SNR component processes. However, in 1995, Thomson $et.\ al$ revealed that, with mode-detection schemes which address the problem of spectral leakage, resonances were manifest in the spectrum of the noise-like component of the signal. In particular, those modes which statistical tests deem significant oscillate at the solar-oscillation frequencies.

When observing natural phenomena, the physicist can only control the experimental design regarding his own detection equipment. This leads to seven complications in the analysis.

1. The system might contain a large number of periodic phenomena, which leads to

*PhD student in the Department of Mathematics and Statistics of Queen's University, Jeffery Hall, 48 University Ave., Kingston, ON Canada, K7L 3N6

†Professor in the Department of Mathematics and Statistics of Queen's University, FRSC, PEng., CStat., Jeffery Hall, 48 University Ave., Kingston, ON Canada, K7L 3N6

numerous couplings between component processes. In the time-series output, the presence of these periodic components is obscured.

2. The record length is finite, so the discrete-time Fourier transform (DTFT) is smoothed. The smoothed DTFT is the discrete Fourier transform (DFT).

3. At a given time index, it is often practically impossible to accurately describe the underlying distribution of the process variable.

4. The detection modality is sensitive to signals from processes extraneous to those containing the modal signature.

5. The variance of the random amplitudes may vary over orders of magnitude, so that, in time-domain models, the majority of low-SNR periodicities are obscured.

6. Non-stationary processes of complicated form introduce spectral power at all frequencies.

7. Periodic components are subjected to external forces, so that their frequencies and phases shift.

This paper shows how techniques from the field of multitaper spectrum estimation can be used to address each of these problems. The problems are addressed as follows.

1. The eigencoefficients of the DFT are defined by harmonics, that coordinate basis which exactly describes the uncoupled oscillations of the system.

2. The eigencoefficients replace the smoothing of a discrete DFT with kernels whose spectral leakage is substantially lower than that of the Dirichlet kernel.

3. The eigencoefficients are efficiency robust with respect to a complex normal distribution.

4. Extraneous measurements are identified with quadratic discriminant analysis (QDA) and detector flags, and are replaced by interpolation.

5. A multitaper reconstruction of the spectral peaks is used to remove the peaks of high-SNR periodic components. This makes the distribution over frequency of the spectral power more uniform across the principle band.

6. Multitaper reconstructions of equivalent-autoregressive (AR) and baseline-noise transfer functions are divided out from the residual spectrum.

7. The efficiency-robustness of the eigencoefficients improves the specificity of a statistical test to distinguish between the modal peaks and the spectrum of the baseline noise process.

## 2. The Dataset

The Geomagnetic Laboratory of Ottawa, Canada [1], has an operational relative ionospheric opacity meter (riometer). The riometer is connected to a radio antenna which points in the zenithal direction to receive cosmic radio noise (Little & Leinbach, 1959). The principle of this detection modality is that the attenuation of cosmic radio noise by the lower ionosphere provides an index of the charge density, and so predictions can be made about the radio-communication conditions. This is especially useful for air flights and satellite missions in the sub-auroral regions, where space weather is a significant source of disruption to electrical systems. When the Sun is not active, the D-region, an ionospheric layer between 50 and 90 km altitude, exhibits a radio-frequency opacity cadence which is, to a first approximation, diurnal. Only at times when the Sun is over the horizon is the region dense with electrons and ions of high energy-absorption cross-section at the radio frequencies. The periodic voltage response which ensues is called the quiet-day curve, and it is subject to logarithmic variations when the Sun is active. Riometer data can also be used to develop the theory of the Earth-space environment. Detection of solar modes in a riometer dataset would be an important discovery because it would progress an understanding of how these modes propagate from the Sun to ground-based detection systems like seismometers (Thomson & Vernon, 2014).

Figure 1 shows the riometer voltage series from 2011. The antenna accepts a continuous feed, $X^{in} = \{X^{in}(t)\}_{t\in\mathbb{R}}$, where each $X^{in}(t)$ is a random variable. The riometer accepts the analogue signal, and it digitizes the signal in the following sequence:

1. The continuous-time signal is passed through a $\Delta t = \frac{1}{60}$ Hz sampler.
2. The decimated signal is passed through a quantizer.
3. The sampled signal is passed through a 60:1 median filter.

As seen in the figure, the ceiling is approximately 7.5 V, and, based on prior knowledge of the temporal structure of absorption events, $\Delta t$ was chosen to reduce aliasing. The voltage response is $\mathbf{X}^{resp} = \{X_n^{resp}\}_{n\in\mathbb{T}}$, where $\mathbb{T} = \{0, \cdots, N-1\}$, and, for $\delta t = 1$s, $X_n^{resp} = X^{resp}(n\,\delta t)$.

## 3. Background

### 3.1 Multitaper Spectrum Estimation

In the model of multitaper spectrum estimation, $X^{in}$ is defined as that continuous-time process whose DTFT Fourier coefficients are $\mathbf{X}^{resp}$ (Percival & Walden, 1998). When truncating the DTFT to a DFT, spectral leakage results from a convolution of the DTFT with the Dirichlet kernel. As seen in Figure 1 of Haley & Thomson, 2014, the periodogram bias can be orders of magnitude. Spectral leakage is reduced by multiplying $\mathbf{X}^{resp}$ with each of a set of discrete, prolate-spheroidal sequences (DPSSs), $\{\mathbf{v}^{(k)}\}_{k=0}^{K-1}$. The DFTs of the filtered series replace the Dirichlet kernel with that set of $K$ kernels, whose spectral energy concentration in the analysis band, $[f-W,\ f+W)$, of the principle alias, $f$, is maximum.

In 1982, Thomson created a spectrum estimator,

[1] The Geomagnetic Laboratory is a government laboratory of Natural Resources Canada. The riometer system was made operational in 2009. Permission to publish results with the riometer data was granted by Donald Danskin of the Geomagnetic Laboratory and David Thomson.

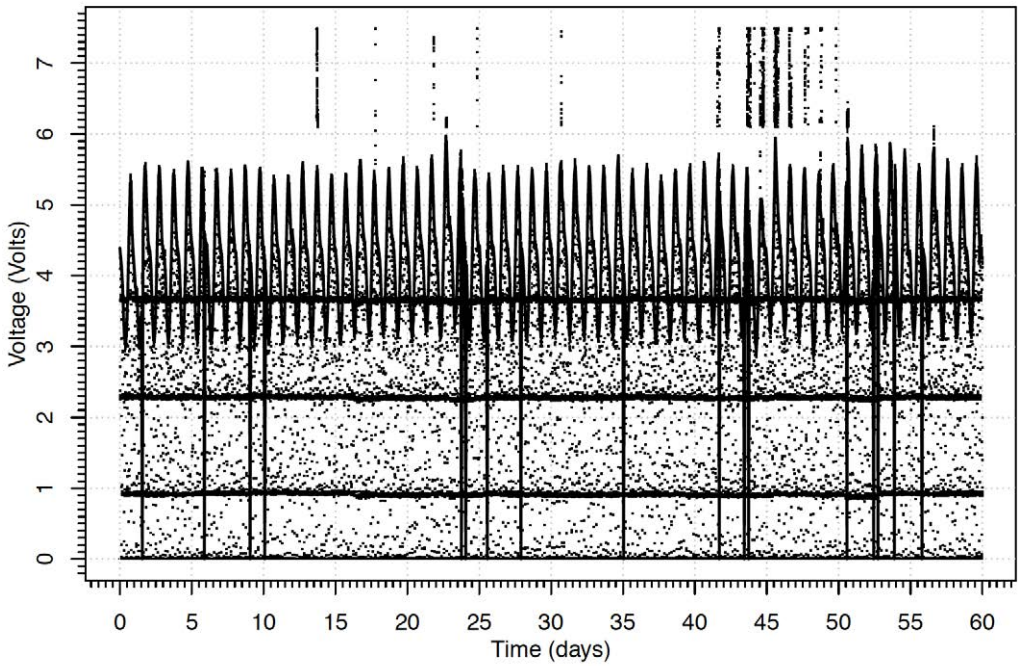


**Figure 1**: The riometer voltage series. A solid, black line crosses samples at every minute of the one-second-sampled voltage series. Isolated black dots above 6.1 V are samples which were identified as extraneous. Black dots below 6.1 V correspond to other extraneous processes, of which the calibration voltages (four, systematic, dark bands below 4 V) contain the vast majority of such samples. The time origin is 34 seconds in to the year, 2011. Data is from the Geomagnetic Laboratory of Ottawa, Canada.

$$\hat{S}^{mt}(f) = \frac{1}{2NW} \sum_{k=0}^{K-1} \frac{1}{\lambda_k} |Y_k(f)|^2, \tag{1}$$

which, for weakly-stationary, locally-white processes is consistent and low-variance. All $\lambda_k \approx 1$, and they are the energy concentrations of the DPSSs in $[f - W,\ f + W)$. The $Y_k(f)$ are called eigencoefficients.

Consider a weakly-stationary process with spectrum, $S$. The $Y_k(f)$ are efficiency robust because they have high variance efficiency with respect to a complex normal distribution (Martin & Thomson, 1982). In papers which describe the distribution of the $Y_k(f)$, the assumption is made that they are each approximately zero-mean, complex-normal, with variance, $S(f)$. Haley & Thomson, 2014 justify this assumption by citing the central limit theorem (CLT) of Mallows, 1967. However, the first author chooses to justify the distributional assumption based on Rosenblatt, 1961, whose central limit theorem (CLT) for linear processes relies only on a strong mixing condition rather than the property of an independent and identically-distributed forcing process.

In several equations of this paper, the true spectrum of the process enters as the argument of a function. Since it is impossible to acquire observations of the true spectrum, the first author used the invariance principle of maximum-likelihood statistics, which is applicable for the multitaper spectrum estimators of locally-white spectra (see Thomson 1990, Lepage & Thomson, 2014, and Stoica & Sundin, 1999).

### 3.2 The Physical Model

In the standard model of helioseismology, the Sun is assumed to exhibit spherical symmetry and remain in a steady-state, hydrostatic equilibrium (Christensen-Dalsgaard, 2002). Thus, solar pressure-modes ("p-modes"), which are amongst the most prominent in space-physics datasets, are described as having the following pressure value at the space-time coordinate, $s = (r,\, \phi,\, \theta,\, t)$ (Christensen-Dalsgaard, 2002):

$$\mathcal{P}(\mathbf{s}) = \sum_{n,l,m} c_{n,l,m} R(r) Y_l^m(\theta,\, \phi) e^{i2\pi f_{nlm} t}. \tag{2}$$

The mode frequencies, $f_{nlm}$, lie in the bands, $[0.45,\, 5.10]$ mHz (acoustic) and $[5.1,\, 15.3]$ mHz (Thomson $et.\, al$, 2007). Pressure modes couple with the interplanetary magnetic field (IMF) (Thomson $et.\, al$, 1995). Then, the IMF disturbances couple with the charge density in the D-region. En route to Earth, the free oscillations of the IMF are damped, and they also experience forcing. The driving forces may each be approximated with an impulse series (Thornton & Marion, 2004). Thus, for $\{\mathbf{M}_j\}_{j=1}^{J}$ random modulators and $\{\mu_{jh}\}_{j=1,\, h=1}^{J,\, H} \subset \mathbb{C}$, the modulated process at time index, $n \in \mathbb{T}$, is (Thomson $et.\, al$, 2001)

$$X_n^{mod} = \sum_{j=1}^{J} M_{j,\, n} \sum_{h=1}^{H} \mu_{jh} e^{i2\pi f_{jh} n}. \tag{3}$$

## 4. A Test for Mode Detection

### 4.1 The Statistical Model

At time index, $n$, the the process variable of $\mathbf{X}^{resp}$ is

$$X_n^{resp} = \begin{cases} X_n^{sol}, & X > 6.1\,\mathrm{V};\; n \in \mathbb{T} \setminus \mathbb{T}_{cal} \\ X_n, & X \in [3,\, 6]\,\mathrm{V};\; n \in \mathbb{T} \setminus \mathbb{T}_{cal} \\ X_n^{cal}, & X \in [3,\, 6]\,\mathrm{V};\; n \in \mathbb{T}_{cal} \end{cases}, \tag{4}$$

where $\mathbb{T}_{cal} \subset \mathbb{T}$ is the set of calibration intervals. Each calibration interval occurs for a full minute once every hour. In this paper, the focus is on $\mathbf{X}$ because $\mathbf{X}^{mod}$ is one of its component processes. It is evident that the DTFT of the input signal is a spectral measure (see Koopmans, 1974 for a review on the theory of spectral measure). This spectral measure can be decomposed into a discrete part, the spectral function, and a continuous part (Koopmans, 1974). Associated with the continuous part is a spectral density. As a result of this decomposition, $\mathbf{X}$ can be represented by a sum of two processes: a high-SNR component process, which itself is associated with the spectral function; and a low-SNR component process, which itself is associated with the spectral density. The low-SNR component may itself be represented as a sum of two processes: an equivalent autoregressive process and an equivalent error process. Then, the equivalent error process is also the sum of two component processes. The first is a noise-like process, which has a spectrum smooth enough that quantile estimation techniques are valid. It is called the baseline process, as it need not necessarily be purely random noise. The second component is $\mathbf{X}^{mod}$.

### 4.2 A Statistical Test for Normal Modes

By the convolution theorem, the DFT of the multiplication of the equivalent error process with the $k$'th DPSS is $Y_k^{err}(f) = Y_k^{base}(f) + Y_k^{mod}(f)$, where, point-wise $f$,

$$Y_k^{mod}(f) = \sum_{j=1}^{J} \sum_{h=1}^{H} \mu_{jh} M_{jk}(f - f_{jh}). \tag{5}$$

Assuming that the $M_{jk}$ are sufficiently narrow-band, define the estimator,

$$\hat{H}^{mt}(f) = \frac{\hat{S}^{(err,\,mt)}(f)}{2\hat{S}^{(base,\,mt)}(f)}, \tag{6}$$

where $\hat{S}^{(err,\,mt)}(f)$ is a multitaper estimator for the spectrum of the equivalent error process and $\hat{S}^{(base,\,mt)}(f)$ is a multitaper estimator for the spectrum of the baseline process. Invoking Rosenblatt's CLT, and defining the $\mu_{jh}$ and $M_{jk}$ appropriately (see Thomson, $et.\,al$, 2001),

$$2K\,\hat{H}^{mt}(f) \sim \begin{cases} \chi^2_{nc;\,2K,\,\lambda},\ f = f_{jh}, & f = f_{jh} \\ \\ \chi^2_{c;\,2K}, & \text{otherwise.} \end{cases} \tag{7}$$

Thus, $\hat{H}^{mt}(f)$ has a $\chi^2_{mix;\,\epsilon;\,2K;\,\lambda}$ mixture distribution, with the mixture parameter, $\epsilon$, defining the percentage of non-central chi-squared samples, and the non-centrality parameter denoted by $\lambda$. The null hypothesis of the statistical test for normal modes is that, at the principle alias, $f$, no mode is present and the distribution of the power is $\chi^2_{c;\,2K}$.

## 5. Data Analysis

An analysis was performed on the first 60 days of the voltage series to test for the presence of periodicities with the solar-oscillation frequencies. The section length was chosen for three reasons. First, compared with other sections of the voltage series, the number of extraneous measurements in the first sixty days is low (see Figure 1). Second, the quiet-day curve of the first section is more coherent than it is in the other sections of the record. Third, solar-oscillation frequencies vary as a function of solar activity, so that, over the course of twenty days, a fraction of mode frequencies shift more than one Rayleigh resolution (Thomson $et.\,al$, 2007). The 2011 solar-flux series from the Penticton Observatory suggests that this was a year where, with solar activity on the rise, mode shift was not minimal[2].

### 5.1 Data Preparation

In Figure 1, $\mathbf{X}^{sol}$ and $\mathbf{X}^{cal}$ measurements are, respectively, seen as: black dots above 6.1 V; and dark, concentrated bands of dots. Replacing these measurements with reconstructions of $\mathbf{X}$ prevents the extraneous sample observations from contaminating the spectrum estimate of $\mathbf{X}$. This data-cleaning step is necessary because it makes the multitaper estimate for the spectrum of $\mathbf{X}$ resistant (Martin, &Ṫhomson, 1982). To remove the extraneous measurements, a hard-rejection scheme was implemented. The riometer dataset includes flags

[2]Data provided by Ken Tapping at the Dominion Radio Astrophysical Observatory of Natural Resources Canada, in Okanagan Falls, British Columbia, Canada. Permission was granted by David Thomson to publish results based on this dataset.

to indicate when calibrations were performed. Identifying $\mathbf{X}^{sol}$ measurements required classification techniques to decide if certain clusters of 6.1 V up-crossings could be attributed to solar radio signals. The series of 6.1 V up-crossings was interpolated using a QDA fit for five classes of daily number density. An overlay of the occurrence durations of solar-burst events with the fitted density profile shows that there exists a high degree of correlation between density class and burst type[3]. As a result, a significant fraction of the 6.1 V up-crossing measurements were identified as $\mathbf{X}^{cal}$ measurements.

For both $\mathbf{X}^{sol}$ and $\mathbf{X}^{cal}$ measurements, replacement reconstructions were determined using the method of good-neighbours outlined in Appendix A of Thomson $et.\,al$, 2001. For a data gap of length, $N_{gap}$, the frequency mesh for the fast Fourier transform (FFT) had $M = \left[2^{\lfloor \log_2(5N_{gap})\rfloor+1}\right]$ points. The time-bandwidth parameter was chosen to be $5\,N_{gap}W = 3$, and $K = 5$ tapers were used[4]. At each replacement interval of the voltage series, left and right neighbour series were used to test the model fit. Box plots of the jackknifed, arc-tangent transformation of magnitude-squared coherence show that, for most reconstructions, the transformation agrees with the standard normal (Brockwell & Davis, 2013). Also, the Kolmogorov-Smirnov test tends to show agreement with 70% confidence. In addition, jackknifed, multitaper estimates of phase offset show no clear signs of structure, and tend about zero.

The time-series was decimated to two-minute sampling using a 120:1 decimation filter. It was constructed using a linear fit in Slepian functions of the rectangular function, itself defined point-wise $f$ to be $\sqcap\left(\frac{f}{120}\right)$. A benefit of this technique is that there is a limit on the complexity of the fit, since the number of available Slepian functions is bounded by the filter length. Filter design was based on the criteria outlined by Koopmans, 1974: that the frequency response of the filter have low integrated mean-squared error and be non-negative definite. The integrated squared error of the fit is 0.016, while only 0.08% of the energy of the transfer function is from the imaginary component.

### 5.2 Estimation of the Baseline Spectrum: Whitening Techniques

In the remainder of this section, note that, for all mentioned multitaper estimates, the time-bandwidth parameter was set to 5.

Using a multitaper estimate, the variance of the reconstructed series is approximately $18.93\,\mathrm{V}^2$. Most of this variance is due to the process mean, which from a multitaper estimate, is approximately 4.3 V (for a discussion on multitaper mean estimation, see Burr, 2012). As a result, the mean estimate was subtracted from the reconstructed voltage series. The variance of the zero-mean component is dominated by the other high-SNR periodic components. Figure 2 shows a multitaper estimate of the spectrum of the voltage series. The five, high-SNR spectral peaks appear at integral multiples of the sidereal-day frequency, which means that the time dependence of the quiet-day curve is more complicated than a diurnal phenomenon. Also, it appears that the rapid fluctuations in the p-mode bands are structured.

Where line components were significant at the 99.9% level of the $F_{2,\,16}$ harmonic F-distribution, multitaper estimates of the peaks were subtracted from the original eigencoefficients. The resulting spectrum estimate yields a residual-process variance estimate of $0.044\,\mathrm{V}^2$. The multitaper estimate of the residual-process dynamic range is 7.64 orders of

[3]Data was acquired from the 2011 burst lists of Monstein, 2017. Permission was granted by Christian Monstein of ETH Zürich to publish results based on this data.

[4]For the remainder of the paper, $M$ is defined as this operation with different record lengths in place of $5N_{gap}$.

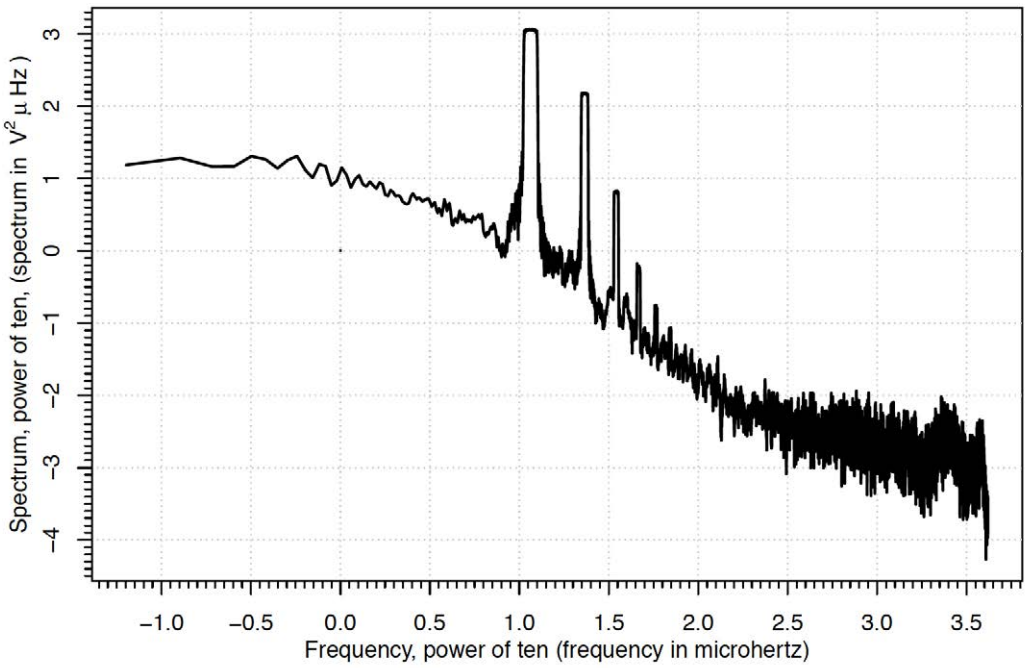


**Figure 2**: A multitaper estimate of the spectrum for the interpolated, one-minute decimated voltage series, after it has been cleaned of extraneous measurements using a hard rejection technique. Parameters for multitaper spectrum estimation were set to $NW = 5$ and $M = \left[2^{\lfloor \log_2(N) \rfloor + 1}\right]$, where $N = 38877$.

magnitude. Using techniques from Thomson $et.\ al$, 2001, the spectrum estimate was divided by an AR-4 transfer function, which yields a multitaper dynamic-range estimate of 3.6 orders of magnitude for the equivalent error process. The multitaper variance estimate for the equivalent error process is $6.6 \times 10^{-3}\,\mathrm{V}^2$.

Optical observations show that, over one-microhertz intervals in the 2-3 mHz band, p-modes have a regular, 100-modes/microhertz density (Thomson $et.\ al$, 2007). As a result, Thomson, et al, 1995 anticipated that, under the alternative hypothesis of solar-mode sinusoids in the equivalent error process, the spectrum of this component should be frequency-homogeneous, in the sense that all powers are samples of the mixture distribution defined by Equation 7. To obtain a piecewise-constant estimate associated with $\hat{S}^{(mt,\,base)}$, the first author implemented the quantile technique of Thomson et al., 2001. For $N = 38,875$, an $M = 38,876$-point FFT mesh was partitioned into $108.1\ \mu$Hz bands, each containing effectively containing one hundred independent samples (Thomson, 2013). Using as an objective function the mean-squared error for empirical quantiles, a grid search was performed to find an optimal $(\lambda,\ \epsilon)$ pair. The theoretical mean-squared error equation was derived from Kendall & Stuart, 1979, and the grid for the parameter space was 100 points on a side. For $(\lambda^*,\ \epsilon^*) = (20,\ 0.4)$, the optimal percentile is 5%. Thus, for each $108.1\ \mu$Hz interval, the estimate of the spectrum for the equivalent error process was divided by the fifth of 100 the ordered samples of that interval.

### 5.3 Results of the Mode-Detection Test

The result of post-whitening is a multitaper estimate of the standardized spectrum, a section of which is presented in Figure 3. Included in the plot are lines at the p-mode frequencies of Broomhall *et. al*, 2009. The figure is to be compared with Figure 4 of Thomson & Vernon, 2015, which itself shows a standardized median spectrum of the time series for the north component of seismic velocity. That time series was obtained from Black Forest Observatory (BFO). Several of the peaks in the riometer spectrum which align with the BFO peaks also happen to be significant at the 99.9% level of the $\chi^2_{18}$ distribution. The $p_{1,10}$ mode is prominent in both spectra, and, in Figure 3, it is the left prong of a noticeable triplet. The splitting of this triplet is caused by a modulation of the mode with the 12 h harmonic of the quiet-day Fourier series. The mode also appears to couple with the 8 h quiet-day harmonic, producing two symmetric peaks on either side of the triplet component. In both spectra, peak structure is similar around the $p_{1,15}$ and $p_{0,16}$ modes, suggesting similar degrees of coupling of solar modes with both the D-region charge density and the seismic velocity.

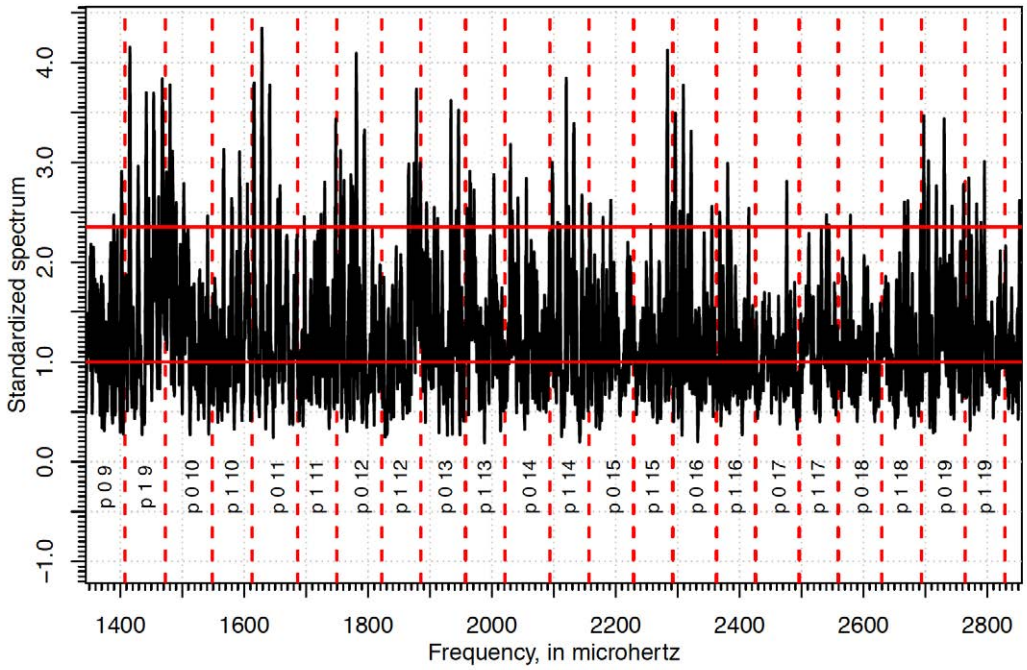


**Figure 3**: Pre- and post-whitened multitaper estimate of the spectrum, standardized to unit value at the 5% level of the central chi-squared distribution with 18 degrees of freedom. The lower, red, horizontal line marks the unit baseline, while the upper, red, horizontal line marks the 99.9% level of the central chi-squared distribution. Red, labeled, vertical lines mark p-mode frequencies from Broomhall et. al, 2009. Labels are of the form, "(l, n)", for $l$ and $n$ respectively the polar and radial order of the solar modes.

## 6. Conclusion

Established techniques of robust multitaper spectrum estimation were used to create a mode-detection test. The result was a discovery of periodic behaviour in the low-SNR component process of a riometer voltage series. Close agreement between mode detections in this paper and those of Broomhall $et.\,al$, 2009 and Thomson & Vernon, 2015 suggests that p-mode oscillations couple with the D-region opacity fluctuatations. The splitting of some of these spectral peaks is conspicuous evidence for the modulation of a sinusoid by the quiet-day Fourier series. Thus, at the 99.9% level of a central chi-squared distribution with 18 degrees of freedom, there is observational evidence to suggest that the $\mathrm{p}_{1,\,10}$ and $\mathrm{p}_{1,\,15}$ modes influence D-region opacity. It is evident from the plot of the standardized spectrum that a significant fraction of the power lies above the 99.9% level of the null distribution. This justifies rejecting the null hypothesis of the noise-like component process being purely random.

## 7. Acknowledgments

The first author is grateful to Dr. David Thomson and Mrs. Maja-Lisa Thomson for their generous support and hours providing advice and direction during the course of this research.

Lenin Arango Castillo of the Economics Department of Queen's helped to improve the quality of this paper, and has participated in valuable discussions about the theory of multitaper spectrum estimation and the research process.

This work was supported by NSERC, CANSSI, Bonneyville Power Authority, and Queen's University. Dr. Thomson, the official holder of the grants and contracts, provided research and conference funding to advance this research project.

Dr. Devon Lin and Dr. Glen Takahara, on the supervisory committee of the first author, have provided significant guidance about the methodology which should be used in the riometer analysis.

At the Geomagnetic Laboratory of Natural Resources Canada, Dr. Donald Danskin and Dr. Robyn Fiori, were generous in providing a large amount of data for analysis. Dr. Danskin has provided a significant amount of advice, and has provided concrete goals for what this analysis is meant to achieve in furthering the advancement of the physics of riometers and ionospheric phenomena. Dr. Christian Monstein (Department of Physics, ETH Zürich), and Dr. Ken Tapping (Dominion Radio Astrophysical Observatory of Natural Resources Canada) provided datasets to help with different stages of the analysis.

Members of Dr. Thomson's research group provided significant input in helping to improve this analysis. Kind thanks to David Reigert, Aaron Springford, Emily Somerset, and Claire Boteler. Dr. Charlotte Haley, Dr. Wesley Burr, Dr. Karim Rahim, and Dr. Joshua Pohlkamp-Hart have provided valuable advice about progressing the analysis.

## REFERENCES


Broomhall, A. M., Chaplin, W. J., Elsworth, Y., & Fletcher, S. T. (2008). The visibility of low-frequency solar acoustic modes. Astronomische Nachrichten, 329(5), 461-469.

Brockwell, P. J., & Davis, R. A. (2013). Time series: theory and methods. Springer Science & Business Media.

Burr, W. S. (2012). Air Pollution and Health: Time Series Tools and Analysis (Doctoral dissertation).

Christensen-Dalsgaard, J. (2002). Helioseismology. Reviews of Modern Physics, 74(4), 1073.

Durbin, J. (1973). Distribution theory for tests based on the sample distribution function. Society for Industrial and Applied Mathematics.

Kendall, M. G., Stuart, A. (1979). The advanced theory of statistics (Vol. 2, Fourth edition). New York: Macmillan Publishing CO., INC.

Koopmans, L. H. (1974). The spectral analysis of time series. New York: Academic press.

Korzennik, Sylvain, "Table of mode parameters", Updated 2017, Viewed 2017, `https://www.cfa.harvard.edu/~sylvain/research/tables/`

Lepage, K. Q., & Thomson, D. J. (2014). Reduced mean-square error quadratic inverse spectrum estimator. IEEE Transactions on Signal Processing, 62(11), 2958-2972.

Little, C. G., & Leinbach, H. (1959). The riometer-a device for the continuous measurement of ionospheric absorption. Proceedings of the IRE, 47(2), 315-320.

Mallows, C. L. (1967). Linear processes are nearly Gaussian. Journal of Applied Probability, 4(2), 313-329.

Thornton, S. T. & Marion, J. B. (2004). Classical dynamics of particles and systems. Academic Press.

Martin, R. D., & Thomson, D. J. (1982). Robust-resistant spectrum estimation. Proceedings of the IEEE, 70(9), 1097-1115.

Monstein, Christian, "e-Callisto International Network of Solar Radio Spectrometers", Updated 2017, Viewed 2017, `http://soleil80.cs.technik.fhnw.ch/solarradio/data/BurstLists/`

Percival, D. B., & Walden, A. T. (1998). Spectral analysis for physical applications. Cambridge University Press.

Rosenblatt, M. (1961). Some comments on narrow band-pass filters. Quarterly of Applied Mathematics, 18(4), 387-393.

Slepian, D. (1983). Some comments on Fourier analysis, uncertainty and modeling. SIAM review, 25(3), 379-393.

Stoica, P., & Sundin, T. (1999). On nonparametric spectral estimation. Circuits, Systems and Signal Processing, 18(2), 169-181.

Thomson, D. J. (1982). Spectrum estimation and harmonic analysis. Proceedings of the IEEE, 70(9), 1055-1096.

Thomson, D. J. (1990). Quadratic-inverse spectrum estimates: applications to palaeoclimatology. Philosophical Transactions of the Royal Society of London A: Mathematical, Physical and Engineering Sciences, 332(1627), 539-597.

Thomson, D. J., Maclennan, C. G., & Lanzerotti, L. J. (1995). Propagation of solar oscillations through the interplanetary medium. Nature, 376(6536), 139.

Thomson, D. J., Lanzerotti, L. J., & Maclennan, C. G. (2001). Interplanetary magnetic field: Statistical properties and discrete modes. Journal of Geophysical Research: Space Physics, 106(A8), 15941-15962.

Thomson, D. J., Lanzerotti, L. J., Vernon, F. L., Lessard, M. R., & Smith, L. T. (2007). Solar modal structure of the engineering environment. Proceedings of the IEEE, 95(5), 1085-1132.

Thomson, D. J. (2013). Background Magnetospheric Variability as Inferred From Long Time Series of Goes Data. Dynamics of the Earth's Radiation Belts and Inner Magnetosphere, 225-242.

Thomson, D. J., & Haley, C. L. (2014, July). Spacing and shape of random peaks in non-parametric spectrum estimates. In Proc. R. Soc. A (Vol. 470, No. 2167, p. 20140101). The Royal Society.

Thomson, D. J., & Vernon III, F. L. (2015). Unexpected, high-Q, low-frequency peaks in seismic spectra. Geophysical Journal International, 202(3), 1690-1710.